Seismoelectric interface electromagnetic wave characteristics for the finite offset Vertical Seismoelectric Profiling configuration

Seismoelectric interface electromagnetic wave characteristics for the finite offset Vertical Seismoelectric Profiling configuration: Theoretical modeling and experiment verification

Yukai Liu
School of Geosciences, China University of Petroleum (East China), Qingdao, China
liuyukai.1008@163.com

David Smeulders
Department of Mechanical Engineering, Eindhoven University of Technology, Eindhoven, Netherlands
d.m.j.smeulders@tue.nl

Yuanda Su and Xiaoming Tang[a)]
School of Geosciences, China University of Petroleum (East China), Qingdao, China
syuanda@sina.com, tangxiam@aliyun.com

Abstract: The seismoelectric interface electromagnetic characteristics have been studied for the finite offset Vertical Seismoelectric Profiling (VSEP) configuration. The approach consists of theoretical modeling and laboratory verification. The results show that the wave variation characteristics along the finite offset measurement line are markedly different from those along the zero-offset line. More interestingly, the wave characteristics for both configurations can be satisfactorily explained by the electric dipole model for the seismoelectric interface wave radiation. Besides, the experiment confirms the modeling result based on the seismoelectric coupling theory and validates the VSEP technique as an effective method for subsurface interface delineation.

[CD]
Date Received: November 7, 2017 **Date Accepted:** December 18, 2017

1. Introduction

Subsurface porous rocks contain electric double layers which, when deformed by passing seismic/acoustic waves, will result in relative movement of the charged ions and generate electromagnetic (EM) signals. This phenomenon is known as seismoelectric effect (Pride, 1994; Pride and Haartsen, 1996). In general, the seismoelectric effect induces two kinds of electric signals. One is the coseismic electric field signal that travels along with the seismic wave. The coseismic signal can only provide localized information around the receivers (Zhu and Toksöz, 2003). Another seismoelectric signal is the interface EM wave, which is generated when the seismic wave impinging onto an elastic or electric interface in the porous medium. Examples of such an interface include rock formation boundary, oil/water contact, and fracture, etc. The seismoelectric interface EM wave propagates or radiates away from the interface with a velocity near the speed of light (Zhu and Toksöz, 2003, 2005; Gao *et al.*, 2017). For such interfaces, the seismoelectric interface EM signal can locate them with the seismic resolution and detect the fluid content using the EM property. Thus, this type of EM signal has great potential in various geophysical applications, such as hydrocarbon exploration and production, ground water contamination, and permafrost interface detection, etc. (Hu *et al.*, 2007; Revil and Jardani, 2010).

Because the seismoelectric interface EM wave is a weak signal and has a relatively low signal-to-noise ratio, the Vertical Seismoelectric Profiling (VSEP) configuration has been used both in the field and laboratory measurements (Dupuis *et al.*, 2009; Schakel *et al.*, 2011; Peng *et al.*, 2017). Similar to Vertical Seismic Profiling, in the VSEP measurements the receiving electrodes are close to the interface of the radiation EM signal generation; this configuration minimizes the propagation loss and can thus improve the signal-to-noise ratio relative to the surface measurements. Depending on

[a)]Author to whom correspondence should be addressed.

the seismic source position relative to the receiving electrodes, the VSEP can be conducted in zero offset and finite offset configurations. Using the finite offset VSEP, Dupuis *et al.* (2009) have conducted the field measurement and analyzed the seismoelectric EM wave amplitude characteristics. In their measurement, the source and electrodes are located at the same side of the interface. For this configuration, however, the first arrival is the coseismic wave which causes a strong interference with the latter small interface EM wave arrival. The interference would be worse in the VSEP measurement where the electrode is close to the interface. Consequently, for the solid-porous model, we can get measurement results at only one side of the interface. Schakel *et al.* (2011) and Peng *et al.* (2017) have measured the response characteristics of the seismoelectric interface EM wave using the fluid-porous model in the laboratory. Because there is no seismoelectric coupling in water, the fluid-porous model can avoid the interference caused by the large amplitude coseismic waves and allows for measuring the pure seismoelectric interface EM wave. Following the work of these researchers for the zero-offset VSEP, this study conducts research for the finite offset VSEP configuration, because the latter configuration is more relevant for subsurface geophysical measurements.

In what follows, we first model the seismoelectric interface EM wave response for the fluid-porous model using the Pride (1994) theory for seismoelectric coupling. The resulting amplitude characteristics of the signals resemble those of an electric dipole at the interface. To verify the theoretical result, we conduct a controlled laboratory experiment and find that the measurement and the theory are in good agreement. The result of this work not only helps understand the mechanism of the seismoelectric interface phenomenon, but also shows that the finite offset VSEP is an effective way for determining a subsurface interface.

2. Theoretical modeling

2.1 Theory

Pride governing equations (Pride, 1994) are widely used in seismoelectric modeling. The modeling results have been validated in numerous laboratory and field experiments (e.g., Schakel *et al.*, 2011; Dupuis *et al.*, 2009). We use the theory to simulate the seismoelectric interface EM wave response of the fluid-porous sandstone interface due to the incidence of an acoustic wave. It should be noted that, unlike the point acoustic source used by Schakel *et al.* (2011) and Gao *et al.* (2017), we use a finite width pulse acoustic source in order to compare the modeling with experiment. The source can radiate the acoustic beam with a sharp directivity similar to that of the acoustic transducer used in the experiment. This finite width pulse source can be adjusted to generate only the interface EM wave for the analysis, eliminating the interference from the coseismic signals, which would otherwise be generated at the fluid-porous model if a point source is used (Peng *et al.*, 2017).

Figure 1 is the seismoelectric model of the fluid-porous sandstone with a finite width pulse acoustic source. In the Cartesian coordinate system, the acoustic source is located at $(0,\ z_S)$ in the fluid region. The receiving electrodes are evenly distributed along a measurement line penetrating the interface; the horizontal offset of the receiver line is D, indicating the finite offset configuration. Zhang (2004) analyzed this configuration for the elastic wave problem. Following their formulation, we analyze the seismoelectric EM wave using the following equations:

$$\varphi_r(x,z) = \int\int A(k,\omega)R^E(k,\omega)\exp\left[-i(k_z^i z_s - k_z^{Er} z + kx - \omega t)\right]dkd\omega, \tag{1}$$

$$\varphi_t(x,z) = \int\int A(k,\omega)T^E(k,\omega)\exp\left[-i(k_z^i z_s + k_z^{Et} z + kx - \omega t)\right]dkd\omega, \tag{2}$$

where φ_r and φ_t are, respectively, the electrical potentials in the fluid and porous sandstone; x and z are the horizontal and vertical coordinates of the receiver; z_S is the distance of the acoustic source to the interface. $k_1 = \omega/V_f$ is the fluid acoustic wavenumber, and V_f is the acoustic velocity. k and $k_z^i = \sqrt{k_1{}^2 - k^2}$ are the horizontal and vertical acoustic wavenumbers, respectively. $A(k,\omega) = \exp[-(k-k_0)^2/k_b^2] * S(\omega)$ is the acoustic source frequency-wavenumber spectral function, which controls the source frequency, radiation angle, and radiation beam width; $S(\omega)$ is the acoustic source spectrum and ω is the angular frequency; k_z^{Er} and k_z^{Et} denote the vertical wavenumber of the EM wave in the fluid and the porous rock, respectively; $R^E(k,\omega)$ and $T^E(k,\omega)$ are, respectively, the reflection and transmission coefficients of the seismoelectric interface EM wave, which can be calculated according to Schakel and Smeulders (2010).

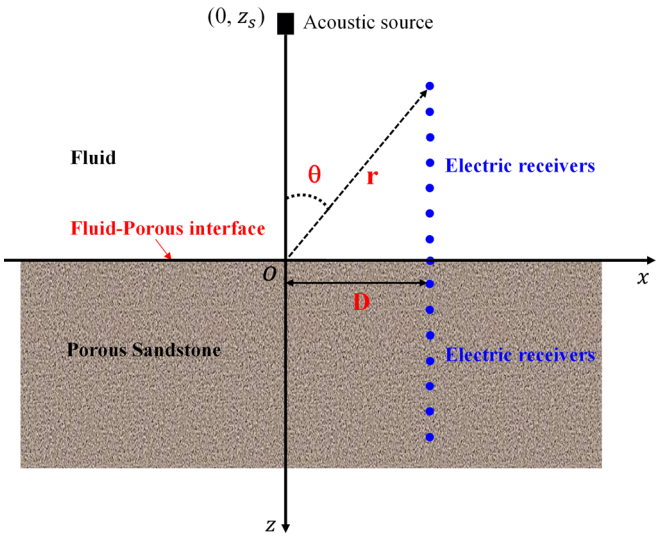

Fig. 1. (Color online) Finite offset VSEP seismoelectric model with a finite width pulse acoustic source.

For a wave incident angle θ, $k_0 = k_1 \sin(\theta)$ determines the radiation direction of the acoustic source; k_b determines the radiation acoustic beam width in space. The role of the exponential function in $A(k, \omega)$ is to insert a two-dimensional bandpass region into the frequency-wavenumber domain of the seismoelectric response function, such that the interface EM signal that falls into this region will be included, whereas other coseismic signals, because their response spectral distribution is outside this region, will be excluded.

2.2 Modeling results and analysis

Using the above-mentioned seismoelectric theory and modeling method, we model the characteristics of the seismoelectric interface EM wave for the finite offset VSEP. The elastic and electrical parameters of the fluid and porous sandstone used in the simulation can be found in Schakel and Smeulders (2010). For the VSEP configuration, the source to interface distance $z_S = 80\,\text{mm}$ and the receiver line offset $D = 45\,\text{mm}$. The receiving electrodes, as shown in Fig. 1, are evenly spaced along the line from $-100\,\text{mm}$ to $100\,\text{mm}$, with $1\,\text{mm}$ spacing. We set the incident angle $\theta = 0^\circ$ and the radiation width $k_b = 80\ \text{mm}^{-1}$ to make the acoustic beam vertically impinge onto the fluid-porous sandstone. A Ricker wavelet with a center frequency $500\,\text{kHz}$ is used for the source function.

Figure 2(a) shows the calculated EM signals along the receiving line. They are colored black, blue, and red when the receiver is above, at, and below the interface, respectively. Three phenomena can be observed from the modeling result. The first is that all signals arrive at a constant time of $T_0 = 52.5\,\mu\text{s}$, which is the acoustic travel time from the source to the interface, indicating that they are the seismoelectric interface EM waves generated by the incident acoustic wave at the interface. The second is the polarity reversal for the signals above and below the interface, which is accompanied by the gradual amplitude variation across the interface. The third phenomenon is that the signal amplitude exhibits a non-monotonic variation on each side of the interface.

The first two phenomena of our finite offset VSEP modeling are similar to those of the zero-offset VSEP experiment (Schakel *et al.*, 2011; Peng *et al.*, 2017). It is the third phenomenon of our modeling that differs greatly from the zero-offset experimental result. (The latter result shows that the signal amplitude monotonically increases toward the interface.) The following analysis is done to reconcile both results.

According to Pride seismoelectric theory (Haartsen and Pride, 1997), the impinging acoustic wave onto the interface of Fig. 1 will generate a vertical electric dipole at the origin O, thereafter the dipole radiates EM waves outward into the whole space with a dipole radiation directivity given by (see Jackson, 1999)

$$\varphi = \mathrm{f}(\mathbf{P}, \varepsilon)\frac{\cos(\theta)}{\mathrm{r}^2}, \tag{3}$$

where φ is the electric potential as a function of distance r (measured from origin) and radiation angle θ (measured from the z axis); $\mathbf{P}$ and ε are, respectively, the electric

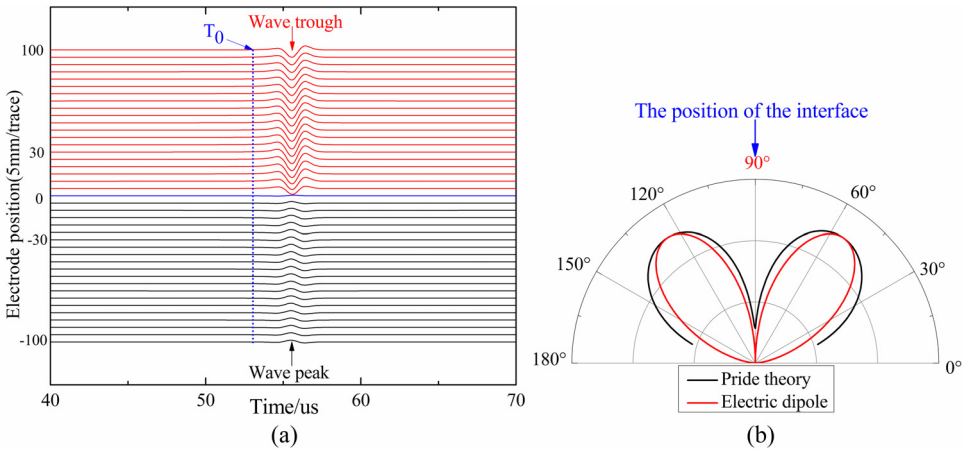

Fig. 2. (Color online) (a) Simulated waveforms of the seismoelectric interface EM wave when the electrodes are located at different positions of the fluid-porous sandstone interface. (b) The modeled (black) electrical potential amplitude variation with the angle θ for the VSEP configuration compared with that of the electric dipole model (red).

dipole moment and the dielectric constant of the medium. For a given medium, $\mathrm{f}(\mathbf{P},\varepsilon)$ is treated as a constant, and the electrical potential radiated from the electric dipole varies with θ and r only, as

$$\varphi \propto \frac{\cos(\theta)}{r^2}. \tag{4}$$

The electric dipole model explains the modeling result of Fig. 2(a) quite well. For the interface located at $\theta = 90^\circ$, the $\cos(\theta)$ function changes signs across the interface. This explains the polarity reversal phenomenon of Fig. 2(a). The modeling data amplitude, after normalization to eliminate the $\mathrm{f}(\mathbf{P},\varepsilon)$ parameter, is compared with that of Eq. (4) in Fig. 2(b), where θ and r for each electrode position can be easily calculated for the configuration in Fig. 1. Figure 2(b) shows that the full modeling result (black) agrees with the dipole model (red) reasonably well. (The slightly fatter pattern of our modeling is presumably caused by the acoustic beam source in the modeling).

The electric dipole model can also explain the result of the zero-offset configuration (Schakel *et al.*, 2011; Peng *et al.*, 2017). For the zero-offset, the source and electrodes are along the same line specified by $\theta = 0^\circ$ $[\cos(\theta) = 1]$, such that $\varphi \propto 1/r^2$, resulting in a monotonic increase of signal amplitude toward the interface as $r \to 0$.

3. Experimental verification

3.1 Experimental apparatus and methods

An experiment was conducted to verify the above theoretical modeling result. The experimental setup is shown in Fig. 3, where a $150 \times 150 \times 110$ mm sandstone block is immersed in a $400 \times 400 \times 400$ mm water tank. The porosity and permeability of the sandstone are 19.7% and 310 mD, respectively. The *p*-wave velocity of the water-saturated sandstone is 3036 m/s at 500 kHz. The water conductivity is 0.5 mS/cm at

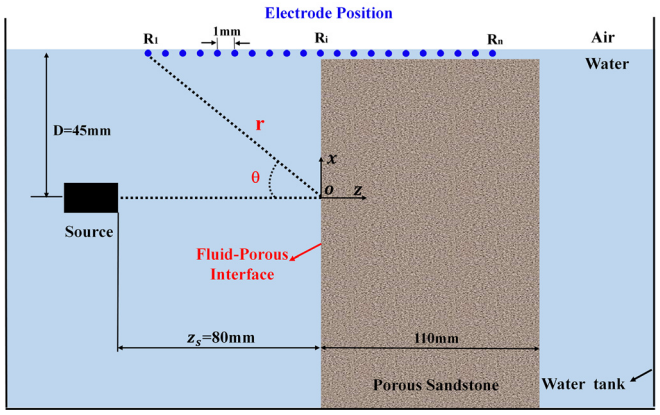

Fig. 3. (Color online) The side view of the experimental measurement setup.

20.2 °C. A 500 kHz center frequency Panametrics, Inc., (Waltham, MA) V391 ultrasonic transducer of 1.125 in. diameter and an A-M system 531 500 electrode (0.008 in. diameter) were used to actuate and receive the seismoelectric signal. The measurement system also includes an Agilent DSO-X-6004A oscilloscope, an Agilent (Santa Clara, CA) 33500B waveform generator, a 50 dB gain Electronic and Innovation (Rochester, NY) 2011L power amplifier, and a 20 dB gain Picotest J2180A preamplifier. In the setup of Fig. 3, the distance between the source and fluid-solid interface is fixed at 80 mm. The distance between the receiving line and the source is $D = 45$ mm. A 500 kHz single cycle sine wave with peak to peak amplitude of 300 V is loaded on the source transducer to actuate the incident acoustic wave.

The electrode measurement positions, which are similar to those in Fig. 1, are shown in Fig. 3. The first electrode position R_1 is placed at 70 mm in front of the interface, the last position R_n is placed at 105 mm behind the interface, and R_i is right at the interface position. By varying the measurement position at 1 mm increment, the angle θ, as defined in Fig. 3, varies from $\theta < 90^\circ$ to $\theta > 90^\circ$, with $\theta = 90^\circ$ coinciding with the interface.

3.2 Experimental results and analysis

To verify that the measured electric signal is the seismoelectric EM signal from the interface, three measurements were made. The first was done by removing the sandstone and placing a Panametrics V391 ultrasonic receiver at the origin O facing the source transducer. The measured acoustic signal serves as a reference signal. The other two measurements were made with the electrode at the R1 position in the presence and absence of the sandstone rock, respectively. The measurement results are shown in Fig. 4(a). It is clear that no electric signal is measured in the absence of the sandstone. In the presence of the rock, the electric (top) and acoustic (bottom) signals occur at the same arrival time of $T_0 = 52.5\,\mu$s, suggesting that the electric signal is generated instantly when the acoustic signal strikes the interface. The former is therefore the seismoelectric EM interface signal radiated from the origin O at the interface at the speed of light in water.

Figure 4(b) shows the measured seismoelectric interface EM signals along the receiving line from left to right (only the section of −70 to 70 mm is shown, at a 5 mm increment). The upper (red) and lower (black) part of the signals were measured for

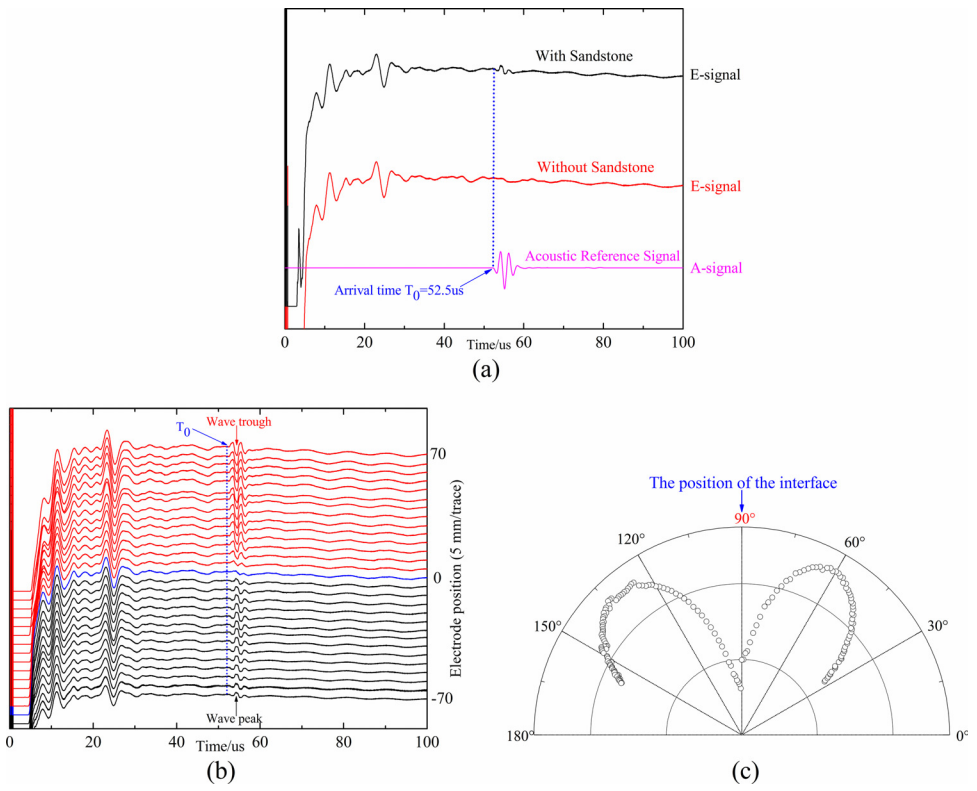

Fig. 4. (Color online) (a) Validation test at receiving position R_1, where the pink (bottom), red (middle), and black (top) signals are the measured acoustic reference signal, electric signal in the absence, and electric signal in the presence, of the sandstone rock, respectively. (b) Measured seismoelectric interface EM waveforms when the electrode is at the different positions of the measurement line. (c) Normalized signal amplitude of (b) versus the angle θ of the electrode position.

positions on right and left of the interface, respectively. For each measurement position, the angle θ and distance r to the origin can be calculated, and the signal amplitude [normalized for each side of the interface to remove the $f(\mathbf{P}, \varepsilon)$ parameter of Eq. (3)] is plotted in Fig. 4(c). (Note the data point in this figure is plotted for every measurement position at an increment of 1 mm.) The pattern of Fig. 4(c) resembles its theoretical counterpart very well. The experiment result is further discussed below.

First, as shown in Fig. 4(b), all signals occur simultaneously at a constant arrival time of $T_0 = 52.5\,\mu$s. For the same reason used to explain in Fig. 4(a), these are the seismoelectric EM waves radiated from the interface. The phase and amplitude variation, especially the polarity reversal phenomenon across the interface, compare very well with the theoretical modeling results in Fig. 2(a). We now analyze the pattern in Fig. 4(c). The peak amplitude position on the left and right side of the interface occur at $\theta = 60^\circ$ and $\theta = 127.5^\circ$, respectively. In comparison, the theoretical value for these two positions are $\theta = 55^\circ$ and $\theta = 125^\circ$, in good agreement with the experimental results. We can therefore conclude that our experiment has verified the seismoelectric EM interface wave characteristics predicted by the Pride (1994) seismoelectric coupling theory.

4. Conclusion

We have studied the seismoelectric interface EM wave phenomenon using the theoretical modeling and laboratory experiment for the finite offset VSEP configuration. We found that the wave variation characteristics along the finite offset measurement line are markedly different from those of the previous zero-offset measurement results. However, the difference can be satisfactorily explained by the electric dipole model for the seismoelectric interface EM radiation. Our experimental result confirms the theoretical modeling result and suggests that the VSEP is a valid method for subsurface interface delineation.

Acknowledgments

The authors thank the associate editor and reviewers for their constructive comments and suggestions that helped improve the manuscript. This work is supported by the China Scholarship Council (201506450027) and the Fundamental Research Funds for the Central Universities (15CX06016A). Y.L. thanks Dr. Sami Musa, Stijn Tolkamp, Shangjing Guo, and Zhengpeng Zhang for valuable discussions.

References and links

Dupuis, J. C., Butler, K. E., Kepic, A. W., and Harris, B. D. (**2009**). "Anatomy of a seismoelectric conversion: Measurements and conceptual modeling in boreholes penetrating a sandy aquifer," J. Geophys. Res. **114**(B10), B10306, https://doi.org/10.1029/2008JB005939.

Gao, Y., Wang, M., Hu, H., and Chen, X. (**2017**). "Seismoelectric responses to an explosive source in a fluid above a fluid-saturated porous medium," J. Geophys. Res. **122**(9), 7190–7218, https://doi.org/10.1002/2016JB013703.

Haartsen, M. W., and Pride, S. R. (**1997**). "Electroseismic waves from point sources in layered media," J. Geophys. Res. **102**(B11), 24745–24769, https://doi.org/10.1029/97JB02936.

Hu, H., Guan, W., and Harris, J. M. (**2007**). "Theoretical simulation of electroacoustic borehole logging in a fluid-saturated porous formation," J. Acoust. Soc. Am. **122**(1), 135–145.

Jackson, J. D. (**1999**). *Classical Electrodynamics.* (John Wiley Press, New York), Chap. 1.

Peng, R., Di, B., Wei, J., Ding, P., Zhao, J., Pan, X., and Liu, Z. (**2017**). "Experimental study of the seismoelectric interface response in wedge and cavity models," Geophys. J. Int. **210**(3), 1703–1720.

Pride, S. (**1994**). "Governing equations for the coupled electromagnetics and acoustics of porous-media," Phys. Rev. B **50**(21), 15678–15696.

Pride, S. R., and Haartsen, M. R. (**1996**). "Electroseismic wave properties," J. Acoust. Soc. Am. **100**(3), 1301–1315.

Revil, A., and Jardani, A. (**2010**). "Seismoelectric response of heavy oil reservoirs: Theory and numerical modelling," Geophys. J. Int. **180**(2), 781–797.

Schakel, M., and Smeulders, D. (**2010**). "Seismoelectric reflection and transmission at a fluid/porous-medium interface," J. Acoust. Soc. Am. **127**(1), 13–21.

Schakel, M. D., Smeulders, D. M. J., Slob, E. C., and Heller, H. K. J. (**2011**). "Seismoelectric interface response: Experimental results and forward model," Geophysics **76**(4), N29–N36.

Zhang, H. (**2004**). *Theoretical Acoustics* (Higher Education Press, Beijing), Chap. 5.

Zhu, Z., and Toksöz, M. N. (**2003**). "Crosshole seismoelectric measurements in borehole models with fractures," Geophys. **68**(5), 1519–1524.

Zhu, Z., and Toksöz, M. N. (**2005**). "Seismoelectric and seismomagnetic measurements in fractured borehole models," Geophys. **70**(4), F45–F51.